

Acta Crystallographica Section F

**Structural Biology  
and Crystallization  
Communications**

ISSN 1744-3091

Editors: **H. M. Einspahr** and **J. M. Guss**

# **Crystallization, X-ray diffraction analysis and SIRAS/molecular-replacement phasing of three crystal forms of *Anabaena* sensory rhodopsin transducer**

**Lutz Vogele and Hartmut Luecke**

Copyright © International Union of Crystallography

Author(s) of this paper may load this reprint on their own web site provided that this cover page is retained. Republication of this article or its storage in electronic databases or the like is not permitted without prior permission in writing from the IUCr.

**Lutz Vogeley and Hartmut  
Luecke\***

University of California, Irvine, USA

Correspondence e-mail: hudel@uci.edu

Received 3 January 2006

Accepted 7 March 2006

## Crystallization, X-ray diffraction analysis and SIRAS/molecular-replacement phasing of three crystal forms of *Anabaena* sensory rhodopsin transducer

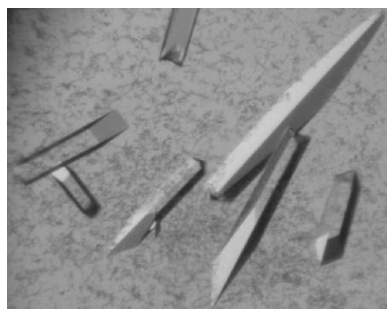
*Anabaena* sensory rhodopsin transducer (ASRT) is a 14.7 kDa soluble signaling protein associated with the membrane-embedded light receptor *Anabaena* sensory rhodopsin (ASR) from *Anabaena* sp., a freshwater cyanobacterium. Crystals of ASRT were obtained in three different space groups, *P*<sub>4</sub>, *C*<sub>2</sub> and *P*<sub>2</sub><sub>1</sub><sub>2</sub><sub>1</sub><sub>2</sub><sub>1</sub>, which diffract to 1.8, 2.1 and 2.0 Å, respectively. Phases for one of these crystal forms (*P*<sub>4</sub>) were obtained by SIRAS phasing using an iodide quick-soak derivative and a partial model was built. Phases for the remaining crystal forms were obtained by molecular replacement using the partial model from the *P*<sub>4</sub> crystal form.

### 1. Introduction

*Anabaena* sensory rhodopsin transducer (ASRT) is a 14.7 kDa soluble protein from the freshwater cyanobacterium *Anabaena* sp. It is co-transcribed with the light-sensing transmembrane protein *Anabaena* sensory rhodopsin (ASR; Vogeley *et al.*, 2004) from a common operon (Jung *et al.*, 2003). Jung and coworkers demonstrated that ASR is a sensory rhodopsin with a relatively slow photocycle ( $t_{1/2} \simeq 110$  ms) and proposed that ASRT is a soluble transducer for the ASR photoreceptor.

ASR is a member of the microbial rhodopsin family. Microbial rhodopsins are membrane-embedded proteins with a retinal chromophore covalently attached *via* a Schiff-base linkage to a lysine in the last of their seven transmembrane helices. The absorption of one photon by the chromophore results in a configurational change at the C<sub>13</sub>=C<sub>14</sub> double bond in the retinal, which in turn triggers a number of conformational changes in the protein that eventually return the photoreceptor to its initial ground state (Lanyi, 2004). Ion-pumping rhodopsins use this photocycle to transport ions across the membrane against electrochemical gradients, while sensory rhodopsins such as ASR use these structural changes for signaling purposes. In the latter case, the structural changes associated with photon absorption are detected by transducer molecules that connect the sensory rhodopsins to signaling cascades involved in the regulation of light-dependent processes. The host of ASR and ASRT, *Anabaena*, is a photosynthetic cyanobacterium in which processes associated with photosynthesis, circadian rhythm control and phototaxis are candidates for regulation by the ASR–ASRT system. Jung *et al.* (2003) demonstrated that ASRT binds to ASR and that its presence speeds up the photocycle of ASR when the two are co-expressed in *Escherichia coli*. This demonstration, the absence of light-induced ion transport by ASR and the fact that the ASR and ASRT genes form one operon are strong indications that ASRT functions as a transducer for ASR.

The only other structurally characterized microbial sensory rhodopsin and transducer system is that of sensory rhodopsin II and its cognate transducer HtrII from the archaeon *Natronomonas pharaonis* (Gordeliy *et al.*, 2002). HtrII is a relatively large protein which contains two transmembrane helices that facilitate the rhodopsin–transducer interaction by forming an intramembrane heterotetrameric complex with two SRII molecules. The eubacterial ASR–ASRT pair represents a completely different signal transduc-



© 2006 International Union of Crystallography  
All rights reserved

tion mechanism involving a small soluble transducer. The archaeal sensory rhodopsins control photoattractant (sensory rhodopsin I) and photophobic (SRII) phototaxis (Spudich *et al.*, 1989), but ASRT lacks the signaling and methylation domains characteristic of taxis signaling proteins. Thus, the ASR–ASRT signal transduction system appears to differ from haloarchaeal sensory rhodopsins both in the nature of its transducer component and with regard to the targeted cellular functions.

## 2. Materials and methods

### 2.1. Expression and purification

Plasmids for expression of C-terminally and N-terminally His-tagged forms of ASRT (Jung *et al.*, 2003) were provided by Professor John Spudich, University of Texas, Houston, USA.

ASRT was overexpressed in *E. coli* BL21 (Novagen, San Diego, CA, USA) grown in Luria–Bertani medium (LB) at 310 K and induced for 4 h with 1 mM isopropyl  $\beta$ -D-thiogalactopyranoside (IPTG). Cell pellets from 4 l culture were resuspended in 30 ml lysis buffer [50 mM Tris–HCl pH 8.0, 300 mM NaCl with 1 mM phenylmethylsulfonyl fluoride (PMSF) and three protease-inhibitor tablets (Roche Diagnostics, Indianapolis, IN, USA)]. Cells were ruptured using a French press. Cell debris and membrane components were removed by centrifugation at 40 000g for 1 h. Remaining fine cell debris was removed by filtration through a 0.22  $\mu$ m syringe filter (Fisher Scientific, Tustin, CA, USA). The protein was purified by FPLC using an Äkta system (Amersham Pharmacia, Piscataway, NJ, USA) and Hi-Trap chelating columns (Amersham Pharmacia, Piscataway, NJ, USA) loaded with Ni<sup>2+</sup>. An imidazole gradient from 10 to 500 mM was used in a running buffer of 30 mM Tris–HCl pH

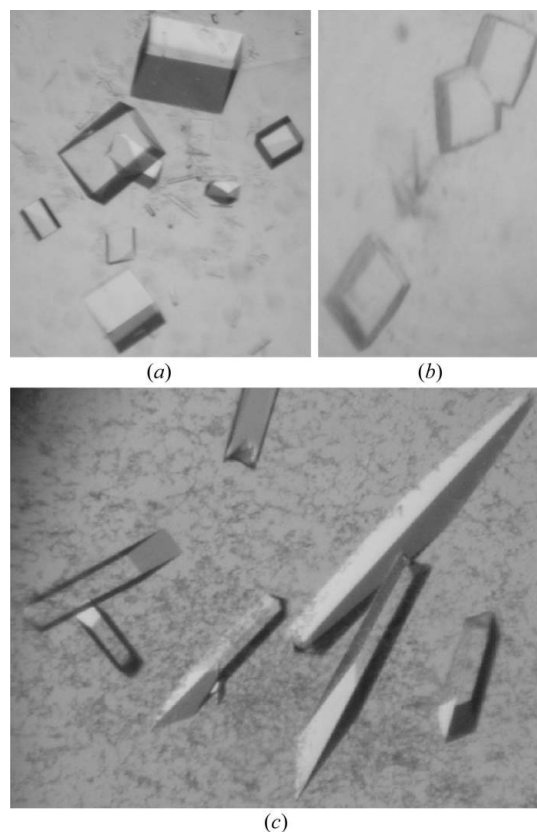


**Figure 1**  
Crystals of ASRT in space groups *P4* (a), *C2* (b) and *P2<sub>1</sub>2<sub>1</sub>2<sub>1</sub>* (c).

**Table 1**

Data-collection statistics for the four crystal forms of ASRT.

Values in parentheses are for the highest resolution shell.

	<i>P4</i>	<i>C2</i>	<i>P2<sub>1</sub>2<sub>1</sub>2<sub>1</sub></i> (small unit cell)	<i>P2<sub>1</sub>2<sub>1</sub>2<sub>1</sub></i> (large unit cell)
Unit-cell parameters				
<i>a</i> (Å)	57.3	85.2	72.8	73.8
<i>b</i> (Å)	57.3	78.8	119.3	122.3
<i>c</i> (Å)	39.8	70.6	120.8	130.1
$\beta$ (°)	90	106.8	90	90
No. of molecules in ASU	1	4	8	8
Matthews coefficient (Å <sup>3</sup> Da <sup>-1</sup> )	2.22	1.93	2.14	2.39
Solvent content (%)	44.7	36.2	42.4	48.5
Data collection				
Resolution (Å)	1.8	2.0	2.1	2.8
Total observations	236749	455390	924424	112315
Unique structure-factor amplitudes	11936	29921	62118	25564
<i>R</i> <sub>merge</sub> (%)	3.1 (21.0)	9.2 (39.8)	3.8 (37.9)	7.3 (36.0)
Average <i>I</i> / $\sigma$ ( <i>I</i> )	33.3 (3.1)	13.8 (2.4)	40.7 (3.9)	12.6 (3.7)
Completeness (%)	98.4 (92.0)	99.0 (94.3)	99.9 (99.8)	85.2 (80.3)
Mosaicity (°)	0.83	0.50	0.40	0.37

**Table 2**

Data-collection and phasing statistics for single-wavelength anomalous dispersion (SAD) data (iodide quick soak).

Values in parentheses are for the highest resolution shell.

Data collection	
Wavelength (Å)	1.541
Resolution (Å)	25–3.0 (3.11–3.00)
No. of unique reflections	4776 (396)
Completeness (%)	97.9 (80.3)
Redundancy	11.3
<i>R</i> <sub>merge</sub> (%)	7.1 (14.0)
Average <i>I</i> / $\sigma$ ( <i>I</i> )	32.8 (14.1)
Unit-cell parameters (Å)	<i>a</i> = 57.2, <i>b</i> = 57.2, <i>c</i> = 39.4
Phasing	
Iodides per ASU	4
<i>f</i> '	–0.31
<i>f</i> ''	6.91
Phasing power (centric/acentric)	0.97/1.32
<i>R</i> <sub>cutis</sub> (centric/acentric/anomalous)	0.65/0.78/0.87
Figure of merit after <i>MLPHARE</i>	0.441
Figure of merit after <i>SOLOMON</i>	0.746

8.0, 300 mM NaCl, 1 mM PMSF. ASRT eluted around 300 mM imidazole. ASRT-containing fractions were dialyzed against 25 mM Tris–HCl pH 8.0, 1 mM PMSF and concentrated to 15 mg ml<sup>-1</sup> using a Centricon 10 kDa cutoff centrifugal filter (Millipore Corporation, Bedford, MA, USA). Sample purity was assessed by SDS–PAGE.

### 2.2. Crystallization and data collection

Initial crystallization conditions were obtained by screening with crystallization kits from Hampton Research (Laguna Niguel, CA, USA) and Emerald Biosciences (Bainbridge Island, WA, USA). Using sitting-drop crystallization with drops of 2  $\mu$ l precipitant solution added to 2  $\mu$ l protein solution over wells containing 200  $\mu$ l precipitant solution at 293 K, three different crystal types were grown over 1–3 weeks (Fig. 1). With the N-terminally His-tagged ASRT, crystals of maximum dimensions 100  $\times$  200  $\times$  350  $\mu$ m grew in the presence of 100 mM sodium acetate pH 4.6 and 7–11% (w/v) polyethylene glycol (PEG) 8000 precipitant solution. These crystals belonged to space group *P4*, with unit-cell parameters *a* = *b* = 57, *c* = 37–40 Å. The C-terminally His-tagged ASRT crystallized in two different space groups. Plate-shaped crystals belonging to space group *C2* (unit-cell parameters *a* = 85.2, *b* = 78.8, *c* = 70.6 Å,  $\beta$  = 106.8°) grew in 100 mM Na<sub>2</sub>HPO<sub>4</sub>, 100 mM citric acid pH 4.2, 35% (v/v) 2-propanol to dimensions of 200  $\times$  200  $\times$  50  $\mu$ m. Crystals belonging to space group *P2<sub>1</sub>2<sub>1</sub>2<sub>1</sub>* formed in 100 mM sodium acetate pH 4.2,

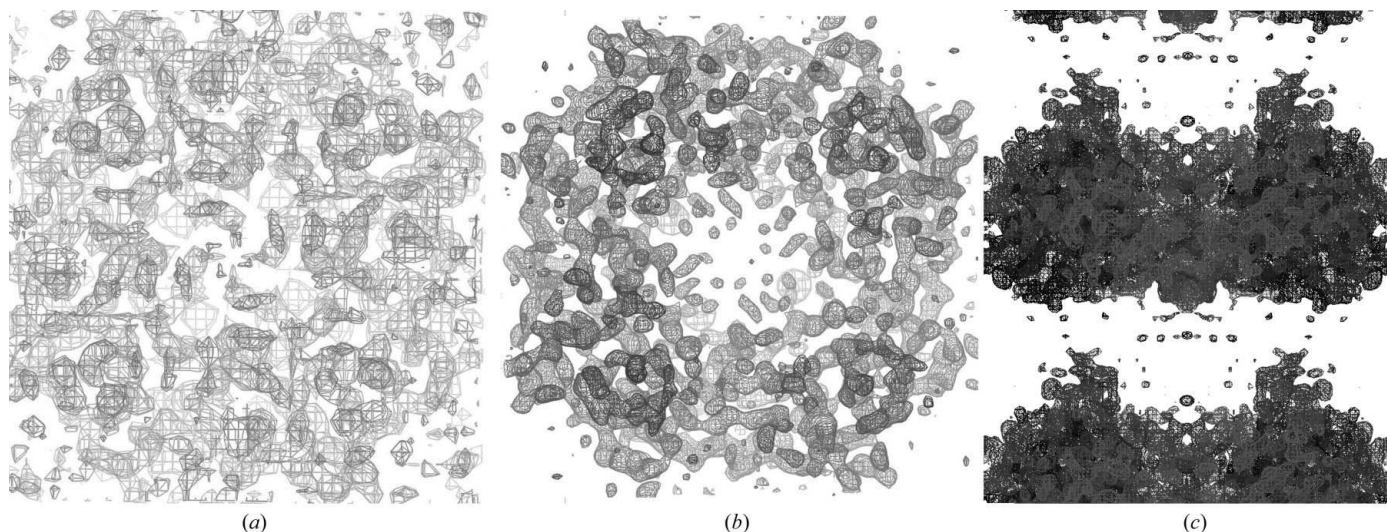


**Figure 2**  
 (a) Experimental electron-density map of one unit cell in the *P4* crystal form after SIRAS phasing using *MLPHARE*. (b) After solvent flipping and solvent flattening using the programs *SOLOMON* and *DM* (both contoured at  $1\sigma$ ). (c)  $2F_o - F_c$  map of the *P4* crystal, covering the crystallographic tetramers in two unit cells stacked along the fourfold axis. The map is contoured at  $1.5\sigma$  to demonstrate the region devoid of electron density which prevents building of a complete model at this point.

10% (w/v) PEG 4000 and grew to  $100 \times 100 \times 700 \mu\text{m}$ . The unit-cell parameters varied from  $a = 73$ ,  $b = 119$ ,  $c = 120 \text{ \AA}$  when cryocooled with 35% (w/v) PEG 4000 as cryoprotectant to  $a = 74$ ,  $b = 122$ ,  $c = 130 \text{ \AA}$  when cryocooled with 20% (v/v) additional glycerol and  $a = 73$ ,  $b = 125$ ,  $c = 135 \text{ \AA}$  at room temperature. At room temperature the  $P2_12_12_1$  crystals only diffracted to  $3.5 \text{ \AA}$  and deteriorated very quickly, so that a complete data set could not be collected.

Diffraction data were collected at the ALS, SSRL and CHESS synchrotrons on crystals cryocooled to 100 K. Raw data were processed with the *HKL2000* suite (Otwinowski & Minor, 1997; Table 1).

### 3. Phase determination

Phases for the *P4* crystal form were determined using the SIRAS technique with an iodide derivative. Crystals were soaked for 20 s in crystallization buffer containing 500 mM potassium iodide. An 11.3-fold redundant  $3.0 \text{ \AA}$  data set was collected on a Rigaku generator with an R-AXIS IV image-plate detector (Table 2). Two iodide sites were found by examination of the Harker section of anomalous difference Patterson maps using the program *XtalView* (McRee, 1999). The program *MLPHARE* (from the *CCP4* suite; Collaborative Computational Project, Number 4, 1994) was used to refine the sites and to locate two additional iodide-binding sites by difference Fourier analysis. SIRAS phasing with *MLPHARE* using the anomalous data set and a  $2.4 \text{ \AA}$  native data set resulted in a mean figure of merit of 0.441. Phases were substantially improved by density modification using the programs *DM* and *SOLOMON* (*CCP4* suite) to give a final figure of merit of 0.746. The resulting electron density was of sufficient quality to allow building of the peptide backbone for 75 out of 125 residues using the programs *MAID* (Levitt, 2001) and *O* (Jones *et al.*, 1990).

This partial model and a new  $1.8 \text{ \AA}$  resolution data set were used with the programs *ARP/wARP* (Perrakis *et al.*, 2001) and *O* to build 89 of the 125 residues of the monomer in the *P4* crystal form. The electron density for the backbone and side chains of these residues is very clear in this crystal form, but there is no density for the remaining 36 residues. 21 C-terminal residues as well as a 12-residue loop do not show any electron density in this crystal form. The

tetramers are stacked along the *c* axis in the *P4* crystal form and the missing loop and C-terminal residues are both located on one end of the tetramer, resulting in  $9 \text{ \AA}$  wide layers with no significant density along the *c* axis between layers of density along the *ab* plane (Fig. 2).

The *C2* and  $P2_12_12_1$  crystal forms were solved by molecular replacement with the partial *P4* model using the *CNS* suite (Brünger *et al.*, 1998). In the meantime, the structural homolog TM1070 had been deposited in the Protein Data Bank (PDB code 1nc7) without an accompanying publication. To date, this entry remains the only structural ASRT homolog in the PDB according to the *DALI* server (Holm & Sander, 1996). Molecular replacement using this structure confirmed the previous results obtained with the partial *P4* structure as the search model. In the *C2* and small unit-cell  $P2_12_12_1$  crystals no significant density beyond the partial search model from the *P4* crystals was observed, but the  $P2_12_12_1$  crystals with the larger unit cell show additional electron density. Refinement of the partial model and efforts to optimize crystallization, cryocooling and data-collection procedures to obtain a more complete model are ongoing.

This work was supported by NIH grant Nos. R01-GM59970 and R01-GM067808. We thank John Spudich, University of Texas, Houston for providing the plasmids for ASRT expression in *E. coli*.

### References

- Brünger, A. T., Adams, P. D., Clore, G. M., DeLano, W. L., Gros, P., Grosse-Kunstleve, R. W., Jiang, J.-S., Kuszewski, J., Nilges, M., Pannu, N. S., Read, R. J., Rice, L. M., Simonson, T. & Warren, G. L. (1998). *Acta Cryst.* **D54**, 905–921.
- Collaborative Computational Project, Number 4 (1994). *Acta Cryst.* **D50**, 760–763.
- Gordeliy, V. I., Labahn, J., Moukhametianov, R., Efremov, R., Granzin, J., Schlesinger, R., Buldt, G., Savopol, T., Scheidig, A. J., Klare, J. P. & Engelhard, M. (2002). *Nature (London)*, **419**, 484–487.
- Holm, L. & Sander, C. (1996). *Methods Enzymol.* **266**, 653–662.
- Jones, T. A., Bergdoll, M. & Kjeldgaard, M. (1990). *Crystallographic and Modeling Methods in Molecular Design*, pp. 189–195. Berlin: Springer-Verlag.
- Jung, K. H., Trivedi, V. D. & Spudich, J. L. (2003). *Mol. Microbiol.* **47**, 1513–1522.
- Lanyi, J. K. (2004). *Annu. Rev. Physiol.* **66**, 665–688.
- Levitt, D. G. (2001). *Acta Cryst.* **D57**, 1013–1019.
- McRee, D. E. (1999). *J. Struct. Biol.* **125**, 156–165.

- Otwinowski, Z. & Minor, W. (1997). *Methods Enzymol.* **276**, 307–326.
- Perrakis, A., Harkiolaki, M., Wilson, K. S. & Lamzin, V. S. (2001). *Acta Cryst.* **D57**, 1445–1450.
- Spudich, E. N., Takahashi, T. & Spudich, J. L. (1989). *Proc. Natl Acad. Sci. USA*, **86**, 7746–7750.
- Vogele, L., Sineschekov, O. A., Trivedi, V. D., Sasaki, J., Spudich, J. L. & Luecke, H. (2004). *Science*, **306**, 1390–1393.